

# Rotation Invariant Convolutions for 3D Point Clouds Deep Learning

Zhiyuan Zhang<sup>1</sup>   Binh-Son Hua<sup>2</sup>   David W. Rosen<sup>1</sup>   Sai-Kit Yeung<sup>3</sup>

<sup>1</sup>Singapore University of Technology and Design   <sup>2</sup>The University of Tokyo

<sup>3</sup>Hong Kong University of Science and Technology

## Abstract

*Recent progresses in 3D deep learning has shown that it is possible to design special convolution operators to consume point cloud data. However, a typical drawback is that rotation invariance is often not guaranteed, resulting in networks that generalizes poorly to arbitrary rotations. In this paper, we introduce a novel convolution operator for point clouds that achieves rotation invariance. Our core idea is to use low-level rotation invariant geometric features such as distances and angles to design a convolution operator for point cloud learning. The well-known point ordering problem is also addressed by a binning approach seamlessly built into the convolution. This convolution operator then serves as the basic building block of a neural network that is robust to point clouds under 6-DoF transformations such as translation and rotation. Our experiment shows that our method performs with high accuracy in common scene understanding tasks such as object classification and segmentation. Compared to previous and concurrent works, most importantly, our method is able to generalize and achieve consistent results across different scenarios in which training and testing can contain arbitrary rotations. Our implementation is publicly available at our project page <sup>1</sup>.*

## 1. Introduction

Recent 3D deep learning has led to great progress in solving scene understanding problems like object classification, semantic and instance segmentation with high accuracies by training a neural network with 3D data. Researches in this area have been continuing to grow and diverse as 3D data becomes more widely and easily available from consumer devices.

Among various data presentations, 3D point cloud is a strong candidate for scene understanding tasks thanks to its availability, compactness, and robustness compared to volumetric or image representations. Point clouds can be acquired by various methods and hardware including mul-

tipple view geometry in dual-lens cameras and structured light or time-of-flight sensing in depth and LiDAR cameras. However, learning with point clouds is deemed challenging because a point cloud does not contain a regular structure such as that in an image or a volume. Performing convolution on point cloud therefore requires some special designs in the convolution operator that takes care of this irregularity. A wide body of works [24, 26, 12, 17, 19, 35, 39, 3] have recently been proposed to solve this problem, demonstrating state-of-the-art performance in scene understanding with point cloud data.

Nevertheless, there remains a fundamental problem with existing convolution operator with point clouds: most previous works do not allow the input point cloud to be *rotation invariant*. During training, data is simply augmented with some rotations which can cause the network not able to generalize well to unseen rotations. A few convolution operators that allows rotation invariance exist [8, 27] but consistent predictions with arbitrarily rotated data are still not achieved.

In this work, we propose a novel convolution operator for point clouds that can achieve high accuracies in scene understanding tasks while still preserving the rotation invariance property. Particularly, our convolution is based on low-level geometric features that are translation and rotation invariant. Such features are used in tandem with a binning approach that addresses point ordering issue in point cloud convolution, resulting in a single convolution that is robust to both issues. In summary, our contributions are:

- A robust feature extraction scheme suitable for convolution that supports both rotation and translation invariant features based on low-level geometric cues;
- A novel convolution operator that is agnostic to both point cloud rotations and point orders. To address the point ordering issue, we devise a simple binning approach that can be seamlessly combined with the feature extraction step;
- A compact convolutional neural network based on the proposed convolution for object classification and object part segmentation. We demonstrate highly consistent and accurate performance under different rotations.

<sup>1</sup><https://hkust-vgd.github.io/riconv/>

## 2. Related Works

The availability of 3D object and scene datasets [36, 41, 2, 11, 6] has made scene understanding in 3D feasible. Common tasks such as object classification, semantic segmentation, and retrieval can now achieve highly accurate results. We briefly summarize the development of 3D deep learning below.

3D deep learning is more diverse compared to image-based deep learning because there are various representations for learning with 3D data. In early stage of 3D deep learning, volume representation [37, 23, 25, 20], or multiple view images [31, 25] are often adopted for neural networks since they are straightforward extensions from learning with images. However, such representations do not scale well due to large memory requirements and limited resolution in representing 3D geometry.

Recently, PointNet [24, 26] sparked the research interest in deep learning with 3D point clouds by showing that it is possible to learn features of a point set with a special network that is robust to input point orders. This opens the capability for object classification and semantic segmentation with point clouds. Several subsequent works are built along this line of research. Alternatives to make convolution operator compatible to point cloud is to summarize point features into a regular grid and apply a traditional convolution [12, 17], performing convolution on a local space such as tangent planes [32], learning to transform point clouds into a canonical latent space [19]. Such techniques perform competitively to PointNet while being able to exploit features from a local region on the point cloud.

The trend of deep learning with point cloud data has been continuing to grow diversely. Recent methods explores convolution kernels that exploit geometric features [30], add edges on top of points [35], parameterize convolution using polynomials [39], and leverage shape context [38]. Some methods are specially design to be lightweight for real-time applications [3], or to combine with recurrent neural network [13] and sequence model [21]. Some methods exploit hierarchical structures and clustering for scalability [28, 15, 33, 34, 16], mapping point cloud to two dimensional space [40, 9, 18], applying spectral analysis [42], or addressing non-uniform point distribution [10].

Our method is a part of this trend. We explore how to perform convolution on local point features and at the same time achieve rotation invariance. Compared to deep learning with images, rotation invariance is an important property and a more critical issue for robustness because in 3D, there is no convention about how to align 3D shapes. In geometric deep learning [4], one can achieve rotation invariance with geodesic convolution on Riemannian manifolds with angular maxpooling [22]. Such convolution, however, needs shape surfaces to operate. By contrast, our convolution is for point sets, and defined directly in the Euclidean space.

The most relevant work to ours is the concurrent work by Rao et al. [27]. They showed that point clouds can be mapped to an icosahedral lattice on which a rotation invariance convolution can be implemented. The key difference here is that we do not need a spherical domain for rotation invariance. Instead, we define convolution with rotation invariant features, which is much simpler and intuitive. In addition, there are a few previous works about learning local descriptors from point clouds for feature matching [43, 14, 7], some of which [7] can be rotation invariant. These works are however orthogonal to ours mainly because they are targeted for point cloud registration.

## 3. Rotation Invariant Convolution

In this section, we detail the RConv operator construction procedure. Our goal is to seek a simple but efficient way to perform traditional convolution on features extracted from an input point cloud. We design a feature extraction scheme such that the local features are invariant to both translation, rotation, and point orders. Different from previous works that rely on a spherical convolution for rotation invariance [8], we show that it is possible to achieve rotation invariance directly in the Euclidean space by utilizing low-level geometric cues.

### 3.1. Rotation Invariant Local Features

Our feature extraction can be explained as in Figure 1. Given a reference point  $p$  (red),  $K$  nearest neighbors are determined to construct a local point set. The centroid of the point set is denoted as  $m$  (blue). We use vector  $\vec{pm}$  as a reference to extract translation and rotation invariant features for all points in the local point set. Particularly, for a point  $x$  in this set, its features are defined as

$$RIF(x; \vec{pm}) = [d_0, d_1, \alpha_0, \alpha_1]. \quad (1)$$

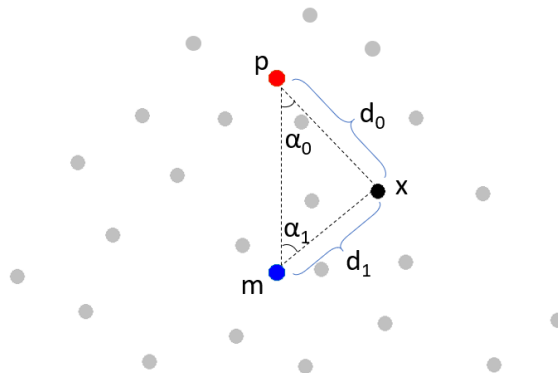


Figure 1. Rotation invariant feature extraction for a point set. At each point (grey), we compute distances and angles to a reference vector established from a reference point (red) and the centroid (blue). Such geometric cues can be directly computed in the Euclidean space, facilitating the design of our convolution operator.

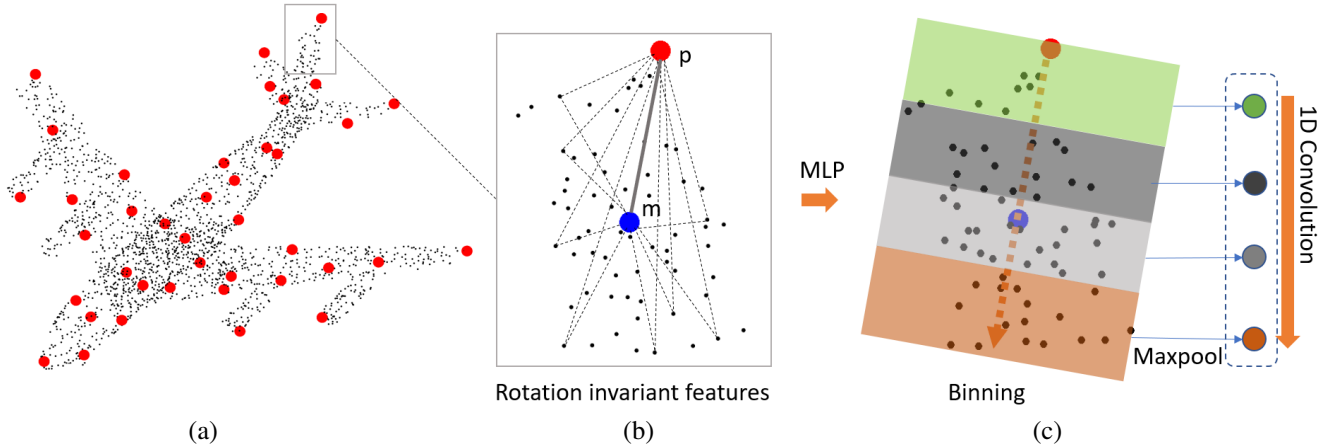


Figure 2. RICConv operator construction. (a) For an input point cloud with/without associated features, representative points (red dots) are sampled via farthest point sampling. (b) For a reference point  $p$ ,  $K$  neighbors are queried to yield a local point set. Also, the centroid of this point set is computed and denoted as  $m$  (blue dot). Vector  $\vec{pm}$  serves as the reference orientation and the point set is transformed into rotation invariant features using the method described in subsection 3.1, which is further lifted to a high-dimensional space by a shared multi-layer perceptron (MLP). (c) The local space is then uniformly divided into several bins along  $\vec{pm}$  and the points of each bin are summarized by maxpooling. Finally, a 1D convolution can be performed to obtain the final features.

Here,  $d_0$  and  $d_1$  represent the distances from  $x$  to  $p$  and to  $m$ , respectively.  $\alpha_0$  and  $\alpha_1$  represent the angles from  $x$  towards  $p$  and  $m$ , as shown in Figure 1. Since such low-level geometric features are invariant under rigid transformations, they are very well suited for our need to make a translation invariant convolution with rotation invariance property. Note that the reference vector  $\vec{pm}$  can also serve as a local orientation indicator and we will use it to build a local coordinate system for convolution, in the subsequent step.

A caveat from the feature extraction scheme is that the reference vector  $\vec{pm}$  can degenerate when  $p$  and  $m$  become a single point. Such cases occur when the neighbors are distributed evenly around the reference point. In such case, we select the farthest point to  $p$  as  $m$  to avoid singularity. In fact, within such a smooth distribution, points that are equidistant to the reference point are expected to have similar features, and thus the degeneration does not negatively affect the features.

### 3.2. Convolution Operator

After obtaining rotation invariant features, we are now ready to detail the main idea of our convolution in Figure 2. A key issue here is how to perform convolution that is agnostic to input point orders. PointNet [24] extracts a global feature vector from the entire input point cloud by maxpooling the features from a shared MLP. Here, we build our convolution on local features and use a binning approach with shared MLP to solve this issue. This idea is relevant to shell based convolution [45] in that both apply binning to resolve the ordering issue of point sets and output fixed size features.

Particularly, we start by sampling a set of representative

points through farthest point sampling strategy which is able to generate uniformly distributed points. From each of which we perform a set of  $K$ -nearest neighbors to obtain local point sets. For each point, the rotation invariant features are extracted as described in the previous section. The features are lifted to a high-dimensional space by a shared multi-layer perceptron (MLP).

To proceed with convolution, we have to define an order so that kernel weights in the convolution can be applied to the corresponding points. Here we devise a simple binning approach and turn the convolution into 1D. Such process has been shown to be highly efficient for local feature learning [45]. In this work, the steps are as follows. We use the reference vector  $\vec{pm}$  and split the point distribution into  $N$  cells along this vector. The feature of each cell is maxpooled from all points participating in the cell. As the cells are ordered, convolution thus becomes possible. We apply a 1D convolution on the fixed-size feature vector from the cells to obtain the output features of our operator. All steps are summarized in Algorithm 1 (see Appendix).

In addition, traditional convolutional neural networks often allows downsampling and upsampling to manipulate the spatial resolution of the input. We build this strategy into our convolution by simply treating the reference point set as the downsampling/upsampling points.

## 4. Neural Networks

We use our convolution operator as the core to build neural networks for two common scene understanding tasks: object classification and object part segmentation. These two tasks are commonly used to benchmark the performance of deep learning with point cloud data [24]. Our network is

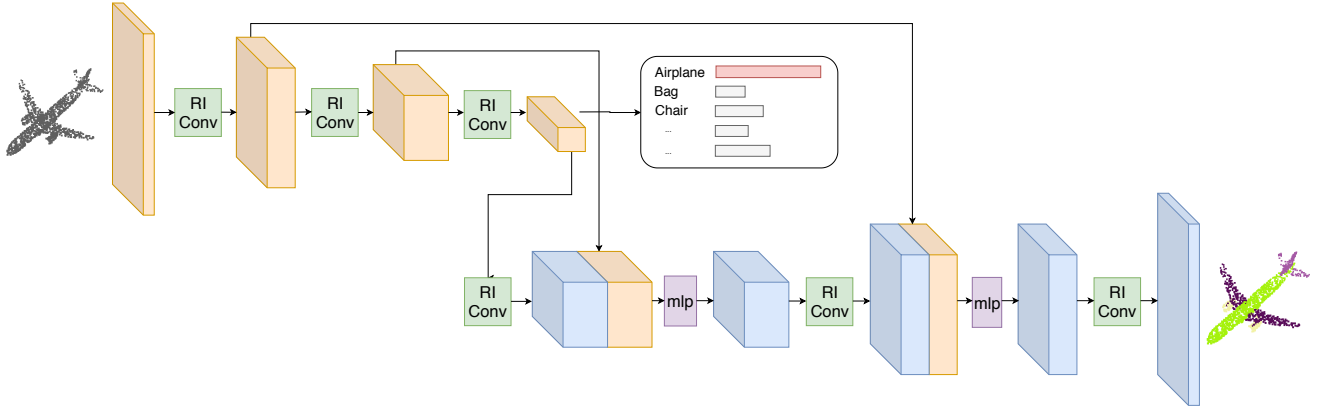


Figure 3. Our proposed network architecture. We follow a convolutional neural network design for classification and part segmentation. Skip connections are further used to combine features from the encoding stage to the decoding stage in part segmentation.

shown in Figure 3.

The object classification network consists of three rotation invariant convolution operators followed by a classifier to output labels for the input point cloud. As our convolution operator is already designed to handle arbitrary rotation and point orders, we can simply place each convolution one after another. By default, each convolution is followed by a batch normalization and an ReLU activation.

The object part segmentation network follows an encoder-decoder architecture with skip connections similar to U-net [29]. We assume a general condition that the object category is unknown when part segmentation is performed. The classification network acts as the encoder, yielding the features in the latent space that can be subsequently decoded into part labels.

In the decoding stage, after each feature is concatenated by skip connections, we apply a MLP before passing the features for deconvolution. Our deconvolution is basically similar to convolution except that it gradually outputs denser points with less feature channels until the output reaches the original number of points.

**Convolution Parameters.** Unless otherwise mentioned, we use 1024 points for classification, and 2048 points for part segmentation, respectively. In the encoding stage, the point cloud is downsampled to 256, 128, and 64, respectively for classification task, and 512, 128, and 32, respectively for segmentation task. The nearest neighbor size is set to 64, 32, and 16 respectively for the three layers of convolutions. We empirically set the number of bins for handling point orders in each convolution as 4, 2, 1, respectively, which strikes a good balance between accuracy and speed. This setting ensures that each bin contains 16 points approximately. In general, the neighborhood has to be large enough for capturing the point distribution and features robustly but not too large that causes too much overhead.

## 5. Experimental Results

We report our evaluation results in this section. We implemented our network in Tensorflow [1]. We use a batch size of 32 for classification training and 16 for segmentation training. The optimization is done with an Adam optimizer. The initial learning rate is set to 0.001. Our training is executed on a computer with an Intel(R) Core(TM) i7-6900K CPU equipped with a NVIDIA GTX 1080 GPU.

We evaluate the proposed convolution and neural network with two tasks: object classification and object part segmentation. The point cloud size is 1024 for classification and 2048 for segmentation. It takes about 3 hours for the training to converge for classification, and about 18 hours for part segmentation. Unless otherwise stated, for object classification, we train for 250 epochs. The network usually converges within 150 epochs. For object part segmentation, we train for 300 epochs, and the network usually converges within 200 epochs.

Following Esteves et al. [8], we perform experiments in three cases: (1) training and testing with data augmented with rotation about gravity axis ( $z/z$ ), (2) training and testing with data augmented with arbitrary SO3 rotations ( $SO3/SO3$ ), and (3) training with data by  $z$ -rotations and testing with data by SO3 rotations ( $z/SO3$ ). The first case is commonly adopted by previous methods in handling rotated point clouds, and the last two cases are for evaluating rotation invariance. In general, it is expected that a convolution with rotation invariance should generalize well in case (3) even though the network is not trained with data augmented with SO3 rotations.

In general, our result demonstrates the effectiveness of the rotation invariant convolution we proposed. Our networks yield very *consistent* results despite that our networks are trained with a limited set of rotated point clouds and tested with arbitrary rotations. To the best of our knowledge, there is no previous work for point cloud learning that is able

Method	Input	Input size	Parameters	$z/z$	SO3/SO3	$z/SO3$	Acc. std.
VoxNet [13]	voxel	$30^3$	0.9M	83.0	<b>87.3</b>	-	3.0
SubVolSup [25]	voxel	$30^3$	17M	88.5	82.7	36.6	28.4
SubVolSup MO [25]	voxel	$30^3$	17M	89.5	85.0	45.5	24.2
Spherical CNN [8]	voxel	$2 \times 64^2$	0.5M	88.9	86.9	78.6	5.5
MVCNN 12x [31]	view	$12 \times 224^2$	99M	89.5	77.6	70.1	9.8
MVCNN 80x [31]	view	$80 \times 224^2$	99M	90.2	86.0	81.5	4.3
PointNet [24]	xyz	$1024 \times 3$	3.5M	87.0	80.3	12.8	41.0
PointNet++ [26]	xyz	$1024 \times 3$	1.4M	89.3	85.0	28.6	33.8
PointCNN [19]	xyz	$1024 \times 3$	0.60M	<b>91.3</b>	84.5	41.2	27.2
Ours	xyz	$1024 \times 3$	0.70M	86.5	86.4	<b>86.4</b>	<b>0.1</b>

Table 1. Comparisons of the classification accuracy (%) on the ModelNet40 dataset. The accuracy is reported on three test cases: training and testing with  $z/z$ , SO3/SO3 and  $z/SO3$  rotation, respectively. Our method has good accuracy and lowest accuracy deviation in all cases.

to achieve the same level of consistency despite that some methods [8] demonstrated good performance when trained with a particular set of rotations. We detail our evaluations below.

### 5.1. Object Classification

The classification task is trained on the ModelNet40 variant of the ModelNet dataset [37]. ModelNet40 contains CAD models from 40 categories such as airplane, car, bottle, dresser, etc. By following Qi et al. [24], we use the pre-processed 9,843 models for training and 2,468 models for testing. The input point cloud size is 1024, with each point represented by  $(x, y, z)$  coordinates in the Euclidean space.

We followed Li et al. [19] and use multiple feature vectors to train the classifier. Particularly, our network outputs 64 feature vectors of length 512 to the classifier. Each of these vectors is passed through an *mlp* implemented by fully connected layers, resulting in  $64 \times 40$  category predictions. During training, we apply cross entropy loss to all such predictions. During testing, we take the mean of such predictions to obtain the final category prediction. In Section 5.3, we further evaluate this strategy and show that it leads to better performance than networks with a single feature vector.

The evaluation results are shown in Table 1. Following the work of [8], we perform experiments in three cases: training and testing with data rotated about the gravity axis ( $z/z$ ), training and testing with arbitrary SO3 rotations (SO3/SO3), and training with  $z$ -rotations and testing with SO3 rotations ( $z/SO3$ ). The first case is commonly adopted by previous methods in handling rotated point clouds, and the last two cases are for evaluating rotation invariance.

We use two criteria for evaluation: accuracy and accuracy standard deviation. Accuracy is a common metric to measure the performance of the classification task. In addition, accuracy deviation measures the consistency of the accuracy scores in three tested cases. In general, it is expected that methods that are rotation invariant should be insusceptible to the rotation used in the training and testing data and therefore

has a low deviation in accuracy.

As can be seen, our method performs favorably to the state-of-the-art techniques. On one hand, our method achieves very good accuracy in all cases despite that there are no clear winner for all cases in our experiment. On the other hand, and more importantly, our method has the lowest accuracy deviation. Previous methods exhibit large accuracy deviations especially in the extreme  $z/SO3$  case. This case is exceptionally hard for methods that rely on data augmentation to handle rotations [24, 26]. In our observation, such techniques are only able to generalize within the type of rotation they are trained with, and generally fail in the  $z/SO3$  test. This applies to both voxel-based and point-based learning techniques. By contrast, our method has almost no performance difference in three test cases, which confirms the robustness of the rotation invariant geometric cues in our convolution. We also evaluate the accuracy of the classification task per object category. Please see the full results in the supplemental document.

**Network Parameters.** The capability to handle rotation invariance also has a great effect on the number of network parameters. For networks that rely on data augmentation to handle rotations, it requires more parameters to ‘memorize’ the rotations. Networks that are designed to be rotation invariant, such as spherical CNN [8] and ours, have very compact representations. In terms of number of trainable parameters, our network has 0.70 millions (0.70M) of trainable parameters, which is the most compact network in our evaluations. Among the tested methods, only spherical CNN [8] (0.5M) and PointCNN (0.6M) have similar compactness. Our network has  $5 \times$  less parameters than PointNet (3.5M), about  $2 \times$  less than PointNet++ (1.4M). The well balance between trainable parameters, accuracy and accuracy deviations makes our method more robust for practical use.

### 5.2. Object Part Segmentation

We also evaluated our method with the object part segmentation task that aims to predict the part label for each

Method	input	SO3/SO3	z/SO3
PointNet [24]	xyz	74.4	37.8
PointNet++ [26]	xyz+normal	<b>76.7</b>	48.2
PointCNN [19]	xyz	71.4	34.7
DGCNN [35]	xyz	73.3	37.4
SpiderCNN [39]	xyz+normal	72.3	42.9
Ours	xyz	75.5	<b>75.3</b>

Table 2. Comparisons of object part segmentation performed on ShapeNet dataset [5]. The mean per-class IoU (mIoU, %) is used to measure the accuracy under two challenging rotation modes: SO3/SO3 and z/SO3.

input point. In this task, we train and test with the ShapeNet dataset [5] that contains 16,880 CAD models in 16 categories. Each model is annotated with 2 to 6 parts, resulting in a total of 50 object parts. We follow the standard train/test split with 14,006 models for training and 2,874 models for testing, respectively.

The evaluation results are shown in Table 2. As can be seen, our method outperforms previous methods significantly in z/SO3 test case and achieves similar performance in SO3/SO3 case. This result aligns well with the performance reported in the object classification task. Our method also has consistent performance for both rotation cases, which empirically confirms the rotation invariance in our convolution. Visualization of our prediction and the ground truth object parts are shown in Figure 4. It is easy to observe that our predictions are the closest to the ground truth. Table 5 and Table 6 further report per-class accuracies for both SO3/SO3 and z/SO3 case. Our method performs best in 3 out of 16 categories in SO3/SO3 case, and 15 out of 16 categories in z/SO3 case.

### 5.3. Evaluations of Network Designs

In this section, we perform experiments on object classification to analyze the performance and justify the design of the proposed convolution operator and network architecture. Inspired by the fact that there are negligible improvement after 150 epochs of training (Section 5.1), we only train the networks with 160 epochs in this ablation study.

**Ablation Study.** We first experiment by turning on/off different components in our network. The result of this experiment is shown in Table 3. In this table, the Base column indicates a simple network similar to that in Figure 3 but only contains RConv operators to extract local features for classification. The MLP indicates the use of an MLP layer to lift rotation invariant features to a high-dimensional feature space. The next two columns indicate the geometric attributes used in RConv. The last row shows that when all components are used, we achieve the best accuracy of 86.5%. Without high-dimensional feature learning by MLP

Base	MLP	Distance	Angle	Acc.
✓		✓	✓	83.4
✓	✓		✓	84.6
✓	✓	✓		84.8
✓	✓	✓	✓	86.5

Table 3. Ablation study of our method. The results show that combining low-level geometric features such as distances and angles lead to better performance. Besides, using MLP for higher dimensional feature learning can also considerably boost the performance.

# Layers	1	2	3	4
Accuracy (%)	46.8	78.2	86.5	86.8
Time per epoch (s)	43.8	59.5	74.5	138.7
# Points	128	256	512	1024
Accuracy (%)	76.0	80.8	84.4	86.5
# Features	Multiple	PointNet style [24]		
Accuracy (%)	86.5	84.8		

Table 4. Classification accuracy (%) with different number of convolution layers, input points, and features for classifiers.

(first row), the performance drops by almost 3%. If we either use angle or distance features (second and third row), the accuracy also drops about 1%. This confirms that our network architecture is plausible and yield good performance.

**Number of Layers.** We vary the number of convolution layers as follows. Let us denote the convolution layers in our network in Figure 3 with  $L_0, L_1, L_2$  from left to right. Here we compare our current architecture with those that have  $L_2$  or  $L_1$  and  $L_2$  removed, or have an additional convolution  $L_{-1}$  added before  $L_0$ . Note that we skip point sampling in  $L_{-1}$  to keep the same number of input points. The results in Table 4 (first section) shows the accuracy when the number of layers vary from 1 to 4. We can see that with only 1 layer, the accuracy drops dramatically to 46.8%, which means a single convolution cannot extract effective features. With more convolutions, the accuracy is improved but this comes with the cost of longer training time. Thus, in this work, we choose the architecture of 3 layers for best speed and accuracy balance.

**Number of Input Points.** We evaluated our network with point clouds of input sizes from 128 to 1024 points. Particularly, we retrained and tested the network with point clouds of corresponding number of points. The results are shown in Table 4 (middle section). It shows that our network generalizes well to different input size.

Network	aero	bag	cap	car	chair	earph.	guitar	knife	lamp	laptop	motor	mug	pistol	rocket	skate	table
PointNet [24]	<b>81.6</b>	68.7	74.0	70.3	87.6	68.5	<b>88.9</b>	80.0	74.9	83.6	56.5	77.6	75.2	<b>53.9</b>	<b>69.4</b>	79.9
PointNet++ [26]	79.5	71.6	<b>87.7</b>	<b>70.7</b>	<b>88.8</b>	64.9	88.8	78.1	79.2	<b>94.9</b>	54.3	<b>92.0</b>	76.4	50.3	68.4	81.0
PointCNN [19]	78.0	80.1	78.2	68.2	81.2	70.2	82.0	70.6	68.9	80.8	48.6	77.3	63.2	50.6	63.2	<b>82.0</b>
DGCNN [35]	77.7	71.8	77.7	55.2	87.3	68.7	88.7	<b>85.5</b>	<b>81.8</b>	81.3	36.2	86.0	77.3	51.6	65.3	80.2
SpiderCNN [39]	74.3	72.4	72.6	58.4	82.0	68.5	87.8	81.3	71.3	94.5	45.7	88.1	<b>83.4</b>	50.5	60.8	78.3
Ours	80.6	<b>80.2</b>	70.7	68.8	86.8	<b>70.4</b>	87.2	84.3	78.0	80.1	<b>57.3</b>	91.2	71.3	52.1	66.6	78.5

Table 5. Per-class accuracy of object part segmentation on the ShapeNet dataset in SO3/SO3 scenario. Our method works equally well to previous methods in this scenario.

Network	aero	bag	cap	car	chair	earph.	guitar	knife	lamp	laptop	motor	mug	pistol	rocket	skate	table
PointNet [24]	40.4	48.1	46.3	24.5	45.1	39.4	29.2	42.6	52.7	36.7	21.2	55.0	29.7	26.6	32.1	35.8
PointNet++ [26]	51.3	66.0	50.8	25.2	66.7	27.7	29.7	65.6	59.7	70.1	17.2	67.3	49.9	23.4	43.8	57.6
PointCNN [19]	21.8	52.0	52.1	23.6	29.4	18.2	40.7	36.9	51.1	33.1	18.9	48.0	23.0	27.7	38.6	39.9
DGCNN [35]	37.0	50.2	38.5	24.1	43.9	32.3	23.7	48.6	54.8	28.7	17.8	74.4	25.2	24.1	43.1	32.3
SpiderCNN [39]	48.8	47.9	41.0	25.1	59.8	23.0	28.5	49.5	45.0	<b>83.6</b>	20.9	55.1	41.7	36.5	39.2	41.2
Ours	<b>80.6</b>	<b>80.0</b>	<b>70.8</b>	<b>68.8</b>	<b>86.8</b>	<b>70.3</b>	<b>87.3</b>	<b>84.7</b>	<b>77.8</b>	80.6	<b>57.4</b>	<b>91.2</b>	<b>71.5</b>	<b>52.3</b>	<b>66.5</b>	<b>78.4</b>

Table 6. Per-class accuracy of object part segmentation on the ShapeNet dataset in z/SO3 scenario. Our method significantly outperforms previous methods thanks to the rotation invariance features from our convolution operators.

**Number of Features for Classifiers.** For object classification, our network outputs 64 vectors of length 512 to the classifier. We compared this strategy with the one in PointNet [24] which only outputs a single vector of 512 by max-pooling all features of all points. The results in Table 4 (last section) shows that more output feature vectors yield slightly higher accuracy. Such boost is due to the fact that multiple vectors can convey richer features from different latent spaces that facilitate feature clustering in the classifier.

## 5.4. Limitations

Our method is not without limitations. First, the geometric features we used is by no means complete. It is possible to use other more sophisticated low-level geometry features such as curvature to design the convolution. Second, while our convolution is robust and consistent to arbitrary rotations, when there is no rotation or simple rotations as in the z/z case in the classification task, our method is less accurate compared to state-of-the-art classification. This is because the original point coordinates are not retained in low-level geometric feature extraction, trading some discriminative features for rotation invariance.

We perform an additional experiment in which we remove the proposed geometric features, and replace them with the original 3D coordinates of the input point cloud. This makes our convolution no longer robust to SO3 rotations but in return, the convolution features are more discriminative. This allows us to achieve state-of-the-art accuracy (91.8% overall accuracy) in the classification task. Fusing original coordinates and geometric features into the same feature space would be therefore a very interesting extension to this work.

## 6. Conclusion

We presented a novel convolution operator for point cloud feature learning that can handle point clouds with arbitrary rotations. Given a point set as input, we determine a reference orientation based on a reference point and the centroid, from which rotation invariant features built upon geometric cues such as distances and angles can be constructed for each point. Combined with a binning strategy, our method handles both rotation invariance and point order issue in a single convolution. We then built a simple yet effective end-to-end convolutional neural network for point cloud classification and segmentation. Experiments demonstrate that our method achieves good performance on both classification and segmentation tasks with the best consistency with arbitrary rotation test cases. This is in contrast to existing methods that often perform quite inconsistently for different types of rotations.

Our method leads to several potential future researches. First, the low-level rotation invariance features for convolution are hand-crafted, which we aim to generalize by applying unsupervised learning to learn such features. Second, our convolution could be beneficial to more scene understanding applications such as object detection and retrieval. It would be also of great interest to extend our method to achieve invariance to rigid and non-rigid transformations.

**Acknowledgement.** The authors acknowledge support from the SUTD Digital Manufacturing and Design Centre (DManD) funded by the Singapore National Research Foundation. This project is also partially supported by Singapore MOE Academic Research Fund MOE2016-T2-2-154 and Singapore NRF under its Virtual Singapore Award No. NRF2015VSGAA3DCM001-014.

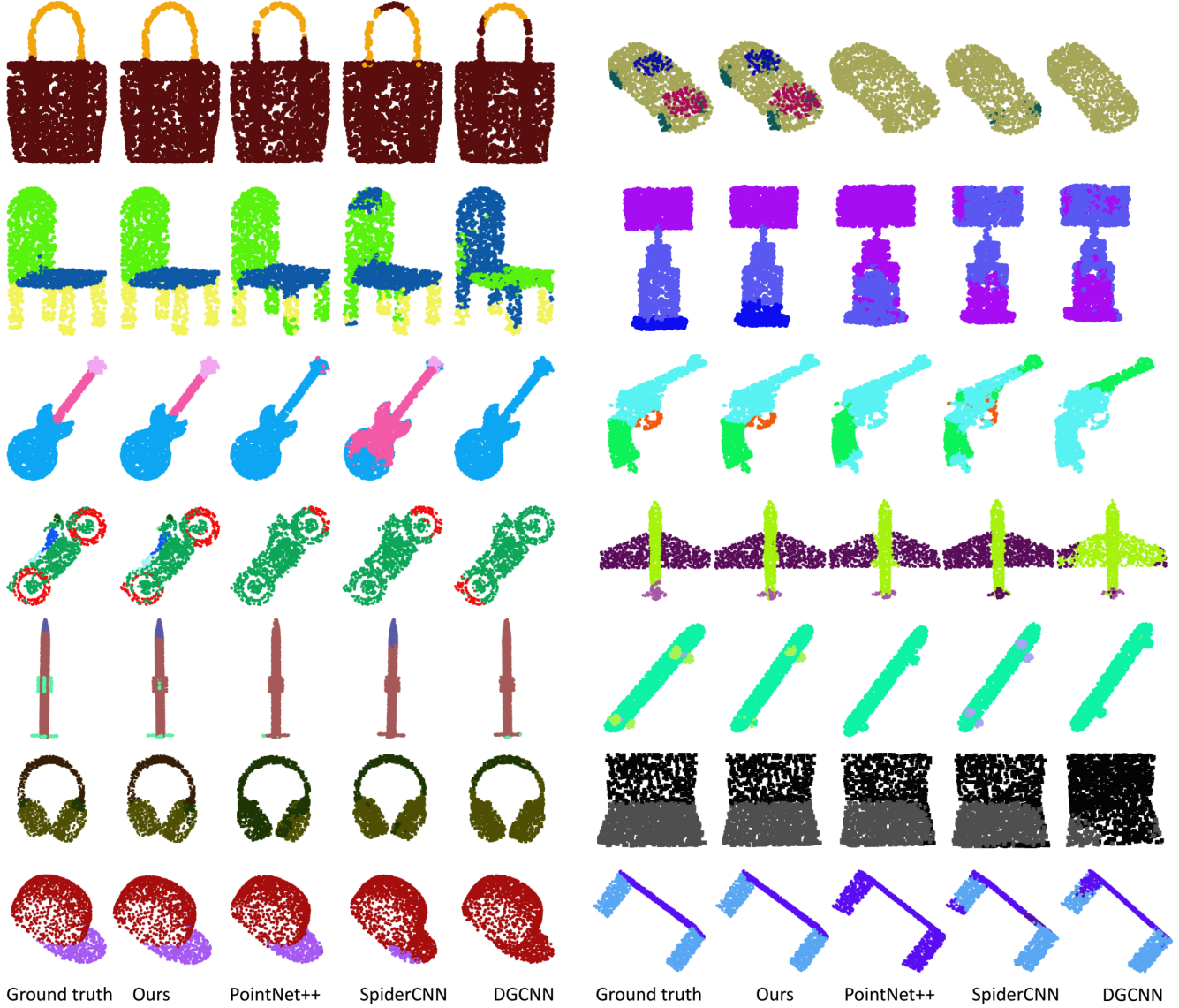


Figure 4. Qualitative results of object part segmentation task with z/SO3 scenario. Our method has the state-of-the-art performance while previous methods fail to generalize to SO3 rotations.

---

**Algorithm 1** RConv operator.

---

**Input:** Reference point  $p$ , point set  $P$ , current point features  $F_{prev}$ ;

**Output:** Convolved features  $F$ ;

- 1:  $m \leftarrow avg(P)$ ;
  - 2:  $\vec{pm} \leftarrow m - p$ ;
  - 3:  $f_r \leftarrow \{RIF(x; \vec{pm}) : \forall x \in P\}$ ;
  - 4:  $F_r \leftarrow mlp(f_r)$ ;
  - 5:  $F_{in} \leftarrow [F_{prev}, F_r]$ ;
  - 6:  $\{S\} \leftarrow P$ ;
  - 7:  $\{F_{pool}\} \leftarrow \{\maxpool(\{F_{in}(x) : \forall x \in s\}) : \forall s \in S\}$
  - 8:  $F \leftarrow conv(\{F_{pool}\})$ ;
  - 9: **return**  $F$ ;
- 

- \* Compute the centroid of  $P$
- \* Determine the reference orientation (Section 3.2)
- \* Find rotation invariant features (Section 3.1)
- \* Transform each feature  $f_r$  to high-dimensional feature  $F_r$
- \* Concatenate the local and previous layer features
- \* Divide local space into  $s$  bins along  $\vec{pm}$
- \* Compute max pooling features for each bin of  $\{S\}$
- \* 1D convolution of the bin features



## References

- [1] M. Abadi, P. Barham, J. Chen, Z. Chen, A. Davis, J. Dean, M. Devin, S. Ghemawat, G. Irving, M. Isard, et al. Tensorflow: A system for large-scale machine learning. In *12th {USENIX} Symposium on Operating Systems Design and Implementation ({OSDI} 16)*, pages 265–283, 2016. 4
- [2] I. Armeni, O. Sener, A. R. Zamir, H. Jiang, I. Brilakis, M. Fischer, and S. Savarese. 3d semantic parsing of large-scale indoor spaces. In *CVPR*, 2016. 2
- [3] Y. Ben-Shabat, M. Lindenbaum, and A. Fischer. 3dmfv: Three-dimensional point cloud classification in real-time using convolutional neural networks. *IEEE Robotics and Automation Letters*, 3:3145–3152, 2018. 1, 2
- [4] M. M. Bronstein, J. Bruna, Y. LeCun, A. Szlam, and P. Vandergheynst. Geometric deep learning: Going beyond euclidean data. *IEEE Signal Processing Magazine*, 34(4):18–42, 2017. 2
- [5] A. X. Chang, T. A. Funkhouser, L. J. Guibas, P. Hanrahan, Q.-X. Huang, Z. Li, S. Savarese, M. Savva, S. Song, H. Su, J. Xiao, L. Yi, and F. Yu. Shapenet: An information-rich 3d model repository. *arXiv preprint arXiv:1512.03012*, 2015. 6
- [6] A. Dai, A. X. Chang, M. Savva, M. Halber, T. Funkhouser, and M. Niessner. Scannet: Richly-annotated 3d reconstructions of indoor scenes. In *CVPR*, pages 5828–5839, 2017. 2
- [7] H. Deng, T. Birdal, and S. Ilic. Ppf-foldnet: Unsupervised learning of rotation invariant 3D local descriptors. In *ECCV*, 2018. 2
- [8] C. Esteves, C. Allen-Blanchette, A. Makadia, and K. Daniilidis. Learning so (3) equivariant representations with spherical cnns. In *ECCV*, pages 52–68, 2018. 1, 2, 4, 5
- [9] T. Groueix, M. Fisher, V. G. Kim, B. Russell, and M. Aubry. AtlasNet: A Papier-Mâché Approach to Learning 3D Surface Generation. In *CVPR*, 2018. 2
- [10] P. Hermosilla, T. Ritschel, P.-P. Vazquez, A. Vinacua, and T. Ropinski. Monte carlo convolution for learning on non-uniformly sampled point clouds. *ACM Transactions on Graphics*, 2018. 2
- [11] B.-S. Hua, Q.-H. Pham, D. T. Nguyen, M.-K. Tran, L.-F. Yu, and S.-K. Yeung. Scenenn: A scene meshes dataset with annotations. In *International Conference on 3D Vision*, 2016. 2
- [12] B.-S. Hua, M.-K. Tran, and S.-K. Yeung. Point-wise convolutional neural network. In *CVPR*, 2018. 1, 2
- [13] Q. Huang, W. Wang, and U. Neumann. Recurrent slice networks for 3d segmentation on point clouds. In *CVPR*, 2018. 2, 5
- [14] M. Khoury, Q.-Y. Zhou, and V. Koltun. Learning compact geometric features. In *ICCV*, 2017. 2
- [15] R. Klokov and V. Lempitsky. Escape from cells: Deep kd-networks for the recognition of 3d point cloud models. In *International Conference on Computer Vision*, pages 863–872, 2017. 2
- [16] L. Landrieu and M. Simonovsky. Large-scale point cloud semantic segmentation with superpoint graphs. In *CVPR*, 2018. 2
- [17] T. Le and Y. Duan. Pointgrid: A deep network for 3d shape understanding. *CVPR*, 2018. 1, 2
- [18] J. Li, B. M. Chen, and G. H. Lee. So-net: Self-organizing network for point cloud analysis. In *CVPR*, 2018. 2
- [19] Y. Li, R. Bu, M. Sun, and B. Chen. Pointcnn: Convolution on x-transformed points. *Advances in Neural Information Processing Systems*, 2018. 1, 2, 5, 6, 7
- [20] Y. Li, S. Pirk, H. Su, C. R. Qi, and L. J. Guibas. Fpnn: Field probing neural networks for 3d data. In *Advances in Neural Information Processing Systems*, pages 307–315, 2016. 2
- [21] X. Liu, Z. Han, Y.-S. Liu, and M. Zwicker. Point2sequence: Learning the shape representation of 3d point clouds with an attention-based sequence to sequence network. In *Association for the Advancement of Artificial Intelligence*, 2019. 2
- [22] J. Masci, D. Boscaini, M. M. Bronstein, and P. Vandergheynst. Geodesic convolutional neural networks on riemannian manifolds. In *The IEEE International Conference on Computer Vision (ICCV) Workshops*, 2015. 2
- [23] D. Maturana and S. Scherer. VoxNet: A 3D Convolutional Neural Network for Real-Time Object Recognition. In *International Conference on Intelligent Robots and Systems*, 2015. 2
- [24] C. R. Qi, H. Su, K. Mo, and L. J. Guibas. Pointnet: Deep learning on point sets for 3d classification and segmentation. In *CVPR*, 2017. 1, 2, 3, 5, 6, 7
- [25] C. R. Qi, H. Su, M. Nießner, A. Dai, M. Yan, and L. J. Guibas. Volumetric and multi-view cnns for object classification on 3d data. In *CVPR*, pages 5648–5656, 2016. 2, 5
- [26] C. R. Qi, L. Yi, H. Su, and L. J. Guibas. Pointnet++: Deep hierarchical feature learning on point sets in a metric space. In *Advances in Neural Information Processing Systems*, pages 5105–5114, 2017. 1, 2, 5, 6, 7
- [27] Y. Rao, J. Lu, and J. Zhou. Spherical fractal convolutional neural networks for point cloud recognition. In *Computer Vision and Pattern Recognition (CVPR)*, 2019. 1, 2
- [28] G. Riegler, A. O. Ulusoy, and A. Geiger. Octnet: Learning deep 3d representations at high resolutions. In *CVPR*, 2017. 2
- [29] O. Ronneberger, P. Fischer, and T. Brox. U-net: Convolutional networks for biomedical image segmentation. In *International Conference on Medical image computing and computer-assisted intervention*, pages 234–241. Springer, 2015. 4
- [30] Y. Shen, C. Feng, Y. Yang, and D. Tian. Mining point cloud local structures by kernel correlation and graph pooling. In *CVPR*, volume 4, 2018. 2
- [31] H. Su, S. Maji, E. Kalogerakis, and E. Learned-Miller. Multi-view convolutional neural networks for 3d shape recognition. In *International Conference on Computer Vision*, pages 945–953, 2015. 2, 5
- [32] M. Tatarchenko, J. Park, V. Koltun, and Q.-Y. Zhou. Tangent convolutions for dense prediction in 3d. In *CVPR*, pages 3887–3896, 2018. 2
- [33] P.-S. Wang, Y. Liu, Y.-X. Guo, C.-Y. Sun, and X. Tong. Ocnn: Octree-based convolutional neural networks for 3d shape analysis. *ACM Transactions on Graphics*, 36(4):72, 2017. 2
- [34] P.-S. Wang, C.-Y. Sun, Y. Liu, and X. Tong. Adaptive ocnn: A patch-based deep representation of 3d shapes. *ACM Transactions on Graphics*, 2018. 2

- [35] Y. Wang, Y. Sun, Z. Liu, S. E. Sarma, M. M. Bronstein, and J. M. Solomon. Dynamic graph cnn for learning on point clouds. *ACM Transactions on Graphics*, 2019. 1, 2, 6, 7
- [36] Z. Wu, S. Song, A. Khosla, F. Yu, L. Zhang, X. Tang, and J. Xiao. 3d shapenets: A deep representation for volumetric shapes. In *CVPR*, pages 1912–1920, 2015. 2
- [37] Z. Wu, S. Song, A. Khosla, F. Yu, L. Zhang, X. Tang, and J. Xiao. 3d shapenets: A deep representation for volumetric shapes. In *CVPR*, pages 1912–1920, 2015. 2, 5
- [38] S. Xie, S. Liu, Z. Chen, and Z. Tu. Attentional shapecontextnet for point cloud recognition. In *CVPR*, 2018. 2
- [39] Y. Xu, T. Fan, M. Xu, L. Zeng, and Y. Qiao. Spidercnn: Deep learning on point sets with parameterized convolutional filters. In *ECCV*, 2018. 1, 2, 6, 7
- [40] Y. Yang, C. Feng, Y. Shen, and D. Tian. Foldingnet: Point cloud auto-encoder via deep grid deformation. In *CVPR*, 2018. 2
- [41] L. Yi, V. G. Kim, D. Ceylan, I.-C. Shen, M. Yan, H. Su, C. Lu, Q. Huang, A. Sheffer, and L. Guibas. A scalable active framework for region annotation in 3d shape collections. *ACM Transactions on Graphics*, 2016. 2
- [42] L. Yi, H. Su, X. Guo, and L. J. Guibas. Syncspecnn: Synchronized spectral cnn for 3d shape segmentation. In *CVPR*, pages 2282–2290, 2017. 2
- [43] A. Zeng, S. Song, M. Nießner, M. Fisher, J. Xiao, and T. Funkhouser. 3DMatch: Learning local geometric descriptors from RGB-D reconstructions. In *CVPR*, 2017. 2
- [44] Z. Zhang, B.-S. Hua, D. W. Rosen, and S.-K. Yeung. Rotation invariant convolutions for 3d point clouds deep learning. In *International Conference on 3D Vision (3DV)*, 2019.
- [45] Z. Zhang, B.-S. Hua, and S.-K. Yeung. Shellnet: Efficient point cloud convolutional neural networks using concentric shells statistics. In *International Conference on Computer Vision (ICCV)*, 2019. 3

# Rotation Invariant Convolutions for 3D Point Clouds Deep Learning Supplementary Material

Zhiyuan Zhang<sup>1</sup> Binh-Son Hua<sup>2</sup> David W. Rosen<sup>1</sup> Sai-Kit Yeung<sup>3</sup>

<sup>1</sup>Singapore University of Technology and Design <sup>2</sup>The University of Tokyo

<sup>3</sup>Hong Kong University of Science and Technology

## Abstract

In this supplementary document, we provide more details about the quantitative and qualitative evaluations presented in the main paper [6]. Particular, we detail convergence plot of testing accuracy/mIoU score over training epochs in the classification and part segmentation task, respectively, to demonstrate the efficiency of our rotation invariance convolution. We report both results in the z/SO3 scenario which is the most challenging case in evaluating rotation invariance convolution. In addition, we also report per-class accuracy in the classification task, and add more visualization results in the object part segmentation task.

## 1. Object Classification

To further demonstrate the benefit of our proposed convolution, we plot the evaluation accuracy against training epochs. The results are shown in Figure 1. In addition, we report per-class accuracy of the classification task in Table 1. As can be seen, we outperforms previous methods significantly. The results of PointCNN [1] is the closest to ours, but in some categories, e.g., desk, laptop, mantel, etc., the results are still less than 50% despite that their convolution also learns a latent transformation. PointNet-based techniques [2, 3] also perform poorly even there are a transformation network learned to rotate the input points into a standard pose. This z/SO3 scenario shows that such transformation networks do not generally adapt well to unseen rotated data.

## 2. Object Part Segmentation

For object part segmentation task, we also detail the capability of generalizing to unseen rotations in our method by plotting the testing mIoU score at different training epochs. The results are in Figure 2. Similar to the observation in the object classification task, it can be seen that our method outperforms previous methods significantly even at early

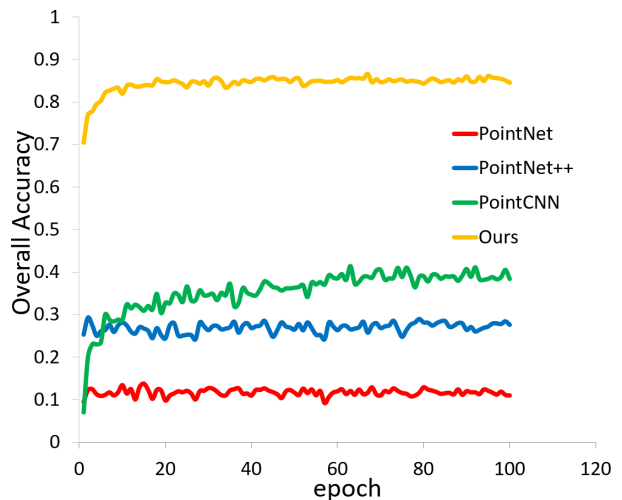


Figure 1. Overall accuracy vs. epochs plot of object classification with z/SO3 scenario. Our method (yellow) is better than PointCNN [1] (green)  $\approx$  10% of accuracy even with early epochs.

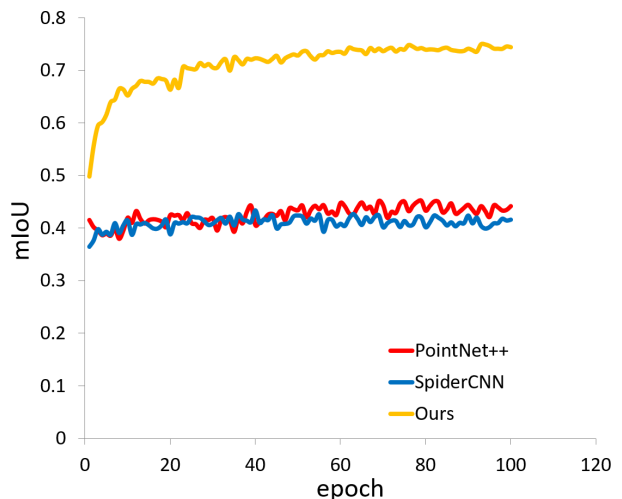


Figure 2. mIoU vs. epochs plot of object part segmentation with z/SO3 scenario. Our rotation invariance convolution outperforms state-of-the-art point cloud learning [3, 5] significantly.

Network	airplane	bathtub	bed	bench	bookshelf	bottle	bowl	car	chair	cone
PointNet [2]	12.0	2.0	8.0	10.0	15.0	14.0	5.0	12.0	9.0	15.0
PointNet++ [3]	53.0	2.0	18.0	10.0	29.0	22.0	20.0	13.0	32.0	20.0
PointCNN [1]	60.0	10.0	20.0	10.0	20.0	37.0	25.0	34.0	46.0	25.0
Ours	<b>100.0</b>	<b>82.0</b>	<b>94.0</b>	<b>80.0</b>	<b>93.0</b>	<b>94.0</b>	<b>100.0</b>	<b>98.0</b>	<b>96.0</b>	<b>90.0</b>
	cup	curtain	desk	door	dresser	flower pot	glass box	guitar	keyboard	lamp
PointNet[2]	0.0	0.0	16.3	5.0	8.1	0.0	4.0	36.0	5.0	15.0
PointNet++ [3]	15.0	45.0	2.3	30.0	9.3	15.0	11.0	47.0	50.0	10.0
PointCNN [1]	15.0	40.0	34.9	30.0	32.6	25.0	35.0	46.0	50.0	20.0
Ours	<b>60.0</b>	<b>95.0</b>	<b>79.1</b>	<b>85.0</b>	<b>73.3</b>	<b>30.0</b>	<b>96.0</b>	<b>99.0</b>	<b>95.0</b>	<b>80.0</b>
	laptop	mantel	monitor	night stand	person	piano	plant	radio	range hood	sink
PointNet [2]	15.0	4.0	11.0	3.5	5.0	36.7	55.0	5.0	4.0	20.0
PointNet++ [3]	15.0	10.0	36.0	1.2	20.0	5.0	71.0	20.0	9.0	5.0
PointCNN [1]	20.0	38.0	35.0	40.7	15.0	34.0	26.0	10.0	28.0	20.0
Ours	<b>95.0</b>	<b>91.9</b>	<b>97.0</b>	<b>77.9</b>	<b>85.0</b>	<b>90.8</b>	<b>83.0</b>	<b>55.0</b>	<b>87.0</b>	<b>75.0</b>
	sofa	stairs	stool	table	tent	toilet	tv stand	vase	wardrobe	xbox
PointNet [2]	11.0	25.0	5.0	3.0	5.0	20.0	4.0	26.3	0.0	10.0
PointNet++ [3]	21.0	10.0	10.0	9.0	15.0	13.0	2.0	<b>85.0</b>	15.0	20.0
PointCNN [1]	32.0	30.0	20.0	36.0	15.0	33.0	29.0	70.0	40.0	15.0
Ours	<b>92.0</b>	<b>85.0</b>	<b>60.0</b>	<b>80.0</b>	<b>70.0</b>	<b>95.0</b>	<b>78.0</b>	76.8	<b>70.0</b>	<b>65.0</b>

Table 1. Per-class accuracy of object classification in z/SO3 scenario with the ModelNet40 dataset [4].

epochs.

Additional visualizations of object part segmentation in shown in Figure 3.

## References

- [1] Y. Li, R. Bu, M. Sun, and B. Chen. Pointcnn: Convolution on x-transformed points. *Advances in Neural Information Processing Systems*, 2018. 1, 2
- [2] C. R. Qi, H. Su, K. Mo, and L. J. Guibas. Pointnet: Deep learning on point sets for 3d classification and segmentation. In *CVPR*, 2017. 1, 2
- [3] C. R. Qi, L. Yi, H. Su, and L. J. Guibas. Pointnet++: Deep hierarchical feature learning on point sets in a metric space. In *Advances in Neural Information Processing Systems*, pages 5105–5114, 2017. 1, 2
- [4] Z. Wu, S. Song, A. Khosla, F. Yu, L. Zhang, X. Tang, and J. Xiao. 3d shapenets: A deep representation for volumetric shapes. In *CVPR*, pages 1912–1920, 2015. 2
- [5] Y. Xu, T. Fan, M. Xu, L. Zeng, and Y. Qiao. Spidercnn: Deep learning on point sets with parameterized convolutional filters. In *ECCV*, 2018. 1
- [6] Z. Zhang, B.-S. Hua, D. W. Rosen, and S.-K. Yeung. Rotation invariant convolutions for 3d point clouds deep learning. In *International Conference on 3D Vision (3DV)*, 2019. 1



Figure 3. Additional qualitative results of object part segmentation task with z/SO3 scenario. Our method has the state-of-the-art performance while previous methods fail to generalize to SO3 rotations.